Title:

Low-dose Radiotherapy Combined with Dual PD-L1 and VEGFA Blockade Elicits Antitumor Response in Hepatocellular Carcinoma Mediated by Activated Intratumoral $CD8^+$ exhausted-like T cells

Supplementary Figures:

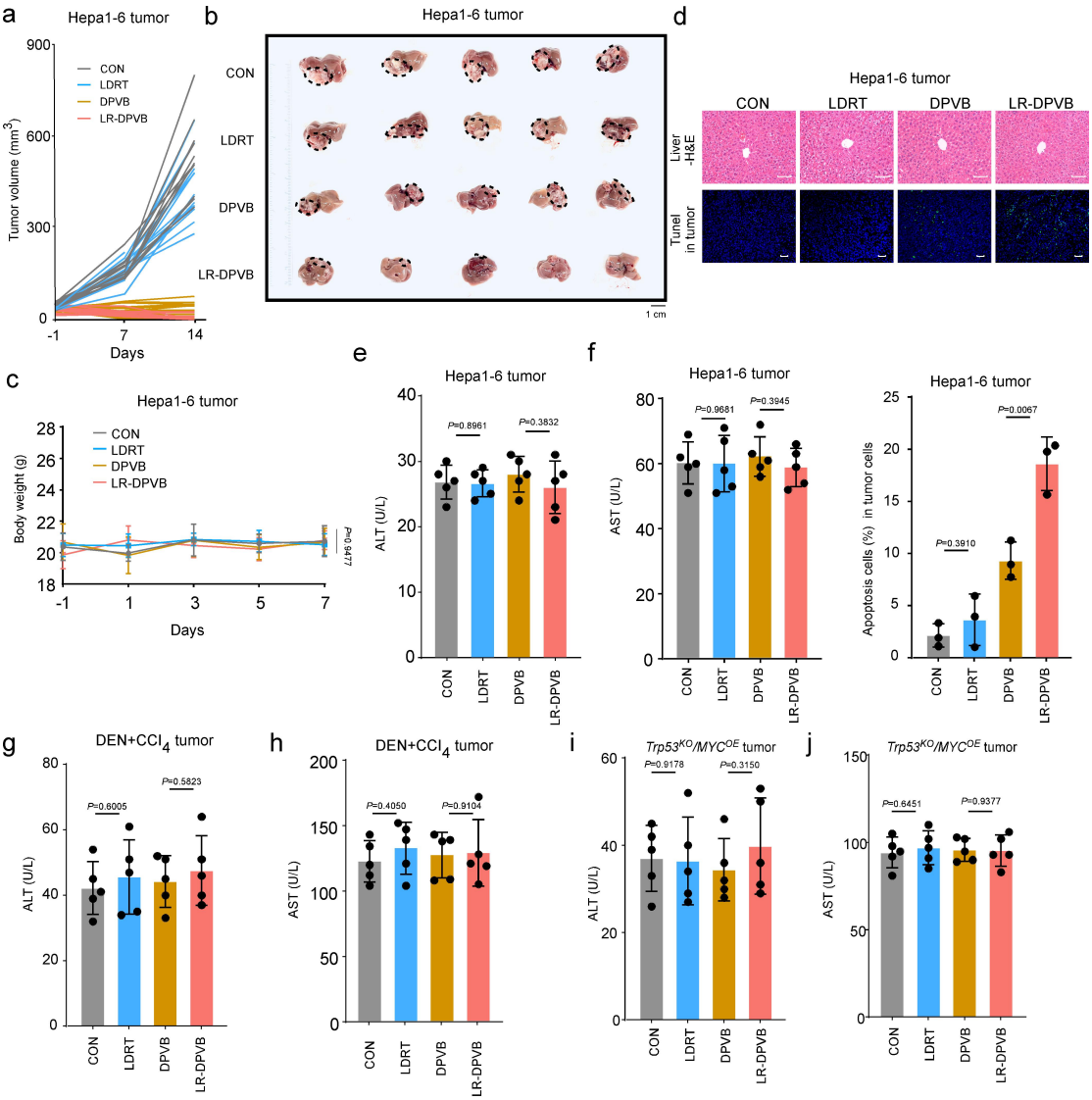

Supplementary Fig. 1 Safety evaluations of combined local liver LDRT in combined with DPVB.

(a) Tumor growth curves of Hepa1-6 HCC model during the therapeutic cycle evaluated by MRI. n=14 mice/group. **(b)** Representative image of Hepa1-6 HCC model at the end of the second therapeutic cycles (circled by black lines). n=5 mice/ group. **(c)** Body weight changes of Hepa1-6 HCC model mice during the two therapeutic cycles. n=5 mice/group. *P* values were calculated using One-way

repeated-measures ANOVA test. **(d)** H&E staining for liver from Hepa1-6 HCC model mice (up) and Tunel assay of Hepa1-6 HCC model liver tumor (down) in each group at the end of the second therapeutic cycles. Quantification of Tunel positive cells in each group. Scale bars: 100 μm. **(e-f)** Serum levels of alanine transaminase (ALT), aspartate aminotransferase (AST) in Hepa1-6 HCC model mice were measured at the end of the second therapeutic cycles. **(g-h)** Serum levels of alanine transaminase (ALT), aspartate aminotransferase (AST) in DEN+CCl_4 HCC model mice were measured at the end of the therapeutic cycles. **(i-j)** Serum levels of alanine transaminase (ALT), aspartate aminotransferase (AST) in *Trp53*^{KO}/*MYC*^{OE} HCC model mice were measured at the end of the therapeutic cycles. Data of **(d)** shown as means ± SD derived from tumor mouse models (n=3 mice/group). Data of **(e-f)** and **(g-j)** shown as means ± SD derived from tumor mouse models (n=5 mice/group). *P* values of **(d-j)** were calculated using a two-sided unpaired Student's *t* test. Source data are provided as a Source Data file.

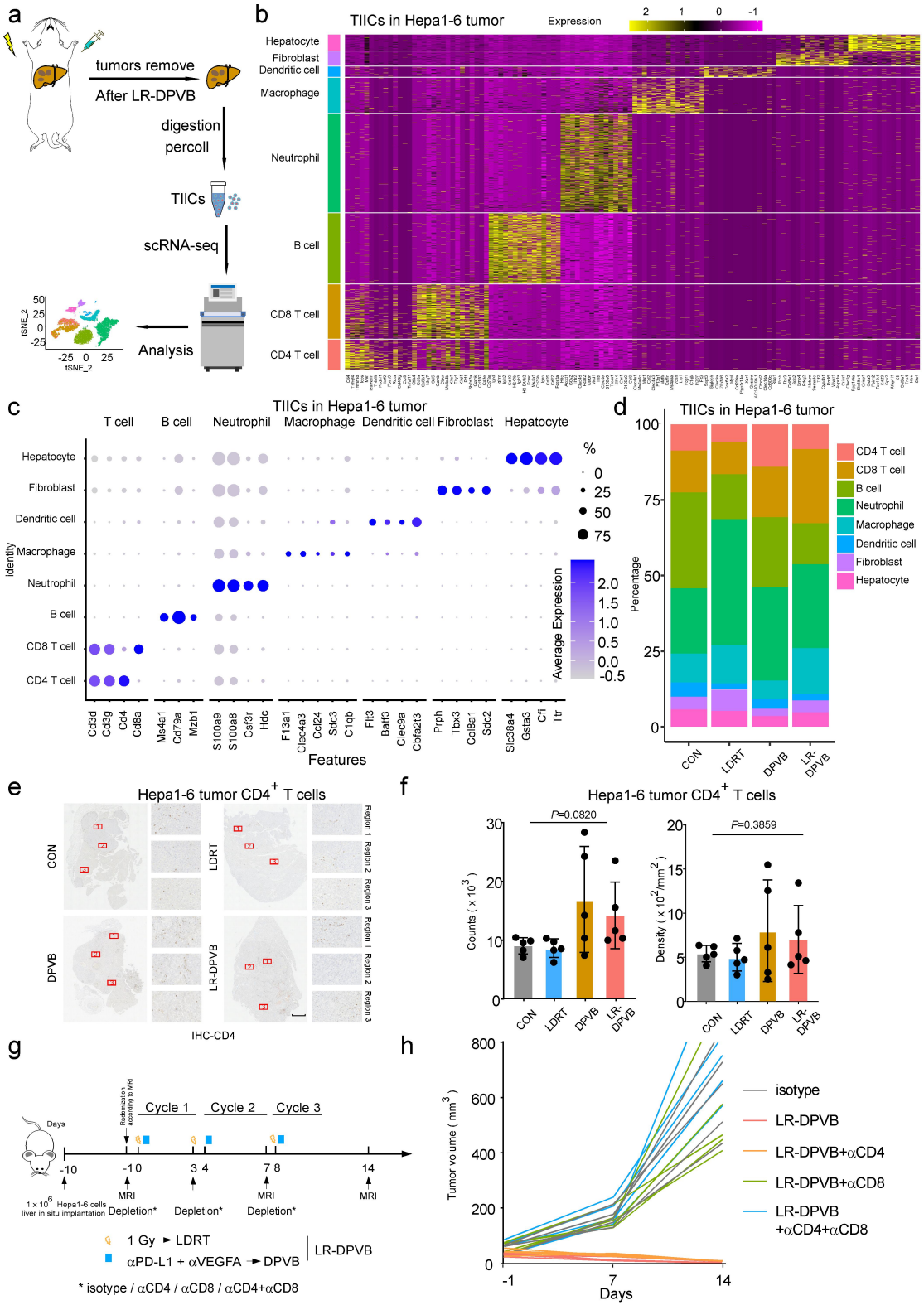

Supplementary Fig. 2 The scRNA-seq characterization of TIICs isolated from Hepa1-6 HCC tumors with 4 different treatment.

(a) The flow chart of single cells isolation and scRNA-seq. n=3 mice/group. **(b)**

Heatmap of display of cell identity marker genes. n=3 mice/group. **(c)** TIICs expressing indicated genes across major cell populations and their corresponding average expression (size of dot indicates the percentage of cells in each population; expression intensity is indicated by color). n=3 mice/group. **(d)** Percentage stack plot representing the proportion of each cell population in different groups. n=3 mice/group. **(e-f)** Representative images **(e)** and quantification **(f)** of CD4 IHC staining in serial sections. n=5 mice/group. *P* values were calculated using a two-sided unpaired Student's *t* test. Data shown as means ± SD. Scale bars: 500 μm. **(g)** Schematic depiction of $CD4^+$ and/or $CD8^+$ T cell depletion experiment in Hepa1-6 bearing LR-DPVB treated mice. **(h)** Tumor growth was assessed at the indicated days. n=5 mice/group. Source data are provided as a Source Data file.

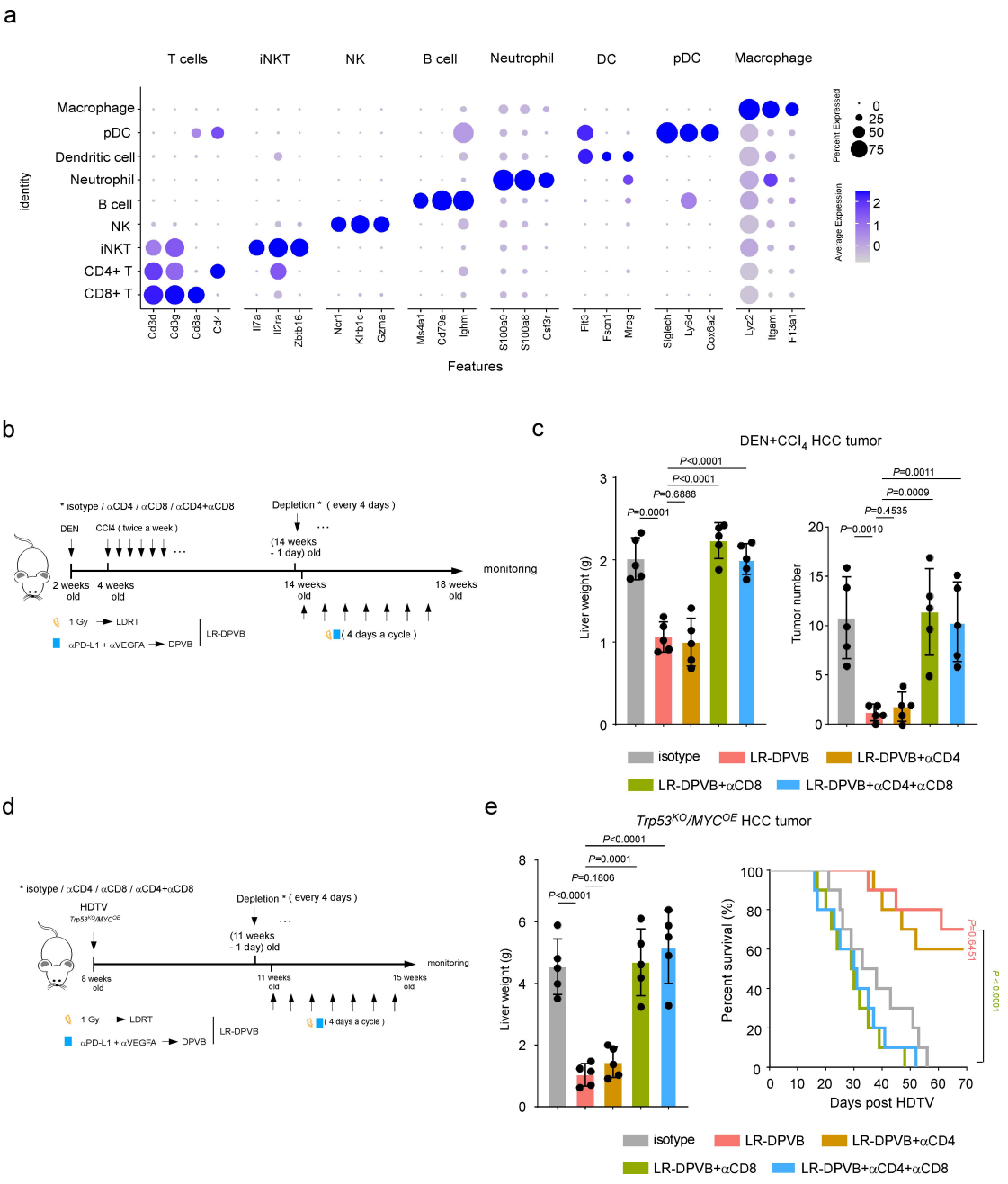

Supplementary Fig. 3 The scRNA-seq characterization of CD45$^+$ TIICs isolated from DEN+CCl$_4$ HCC tumors with 4 different treatment.

(a) CD45$^+$ TIICs expressing indicated genes across major cell populations and their corresponding average expression (size of dot indicates the percentage of cells in each population; expression intensity is indicated by color). n=3 mice/group. **(b)** Schematic depiction of CD4$^+$ and/or CD8$^+$ T cell depletion experiment in DEN+CCl$_4$ HCC mice. **(c)** The liver weight (left panel) and tumor number (right panel) of DEN+CCl$_4$ HCC model at the indicated groups. n=5 mice/group. *P* values were calculated using a

two-sided unpaired Student's *t* test. **(d)** Schematic depiction of $CD4^+$ and/or $CD8^+$ T cell depletion experiment in $Trp53^{KO}/MYC^{OE}$ HCC mice. **(e)** The liver weight (left panel, n=5 mice/group, *P* values were calculated using a two-sided unpaired Student's *t* test) and Kaplan – Meier curve (right panel, n=10 mice/group, *P* values were determined by log-rank test (Mantel-Cox)) of $Trp53^{KO}/MYC^{OE}$ HCC model at the indicated groups. Data of **(c)** and **(e)** shown as means ± SD of derived from tumor mouse models (n=5 mice/group). Source data are provided as a Source Data file.

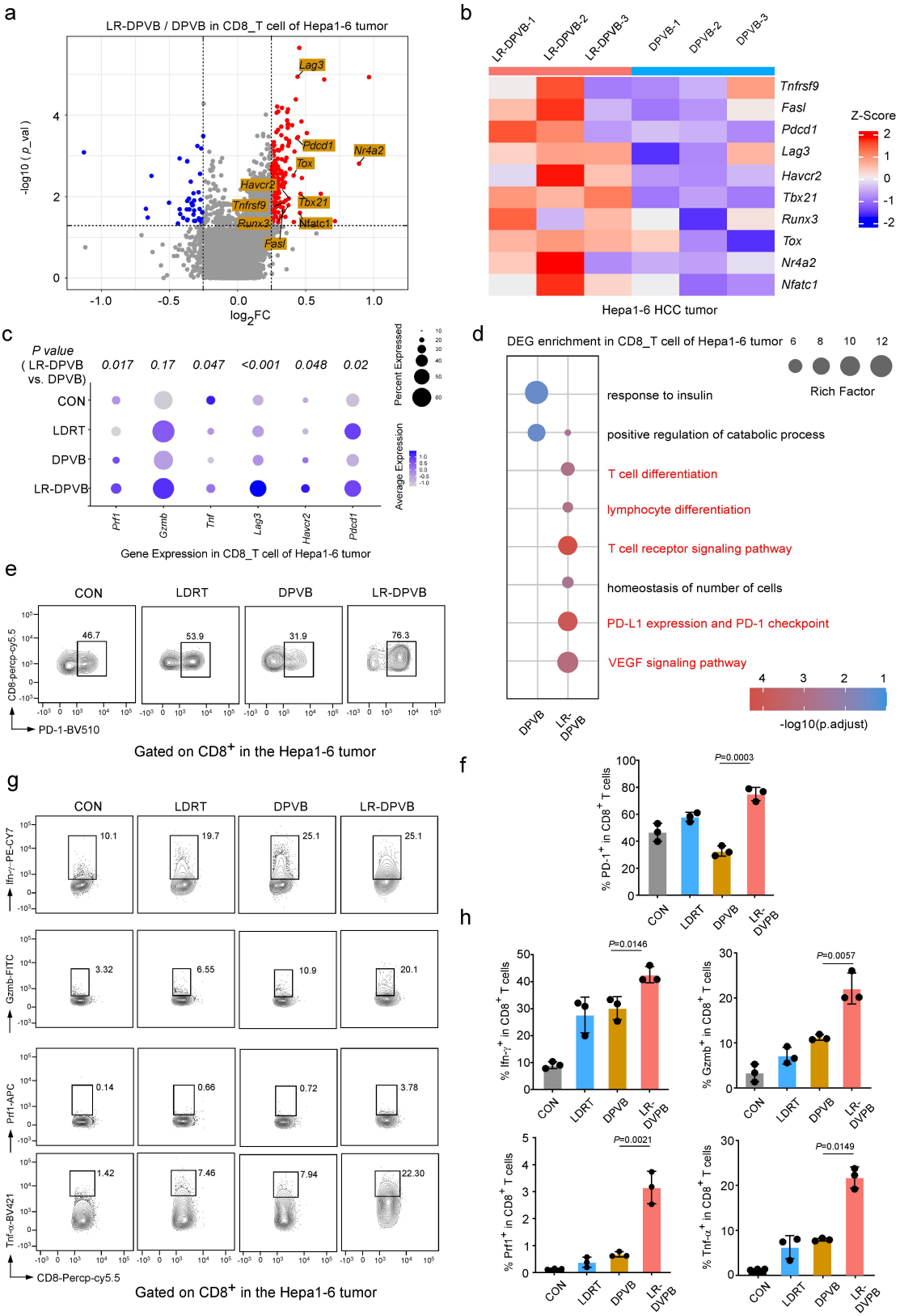

Supplementary Fig. 4 The LR-DPVB expands the exhausted and activated of CD8⁺ T cells in Hepa1-6 HCC tumors.

(a) Volcano plot representing the differentially expressed genes (DEGs) of CD8_T

cells in Hepa1-6 HCC tumor of LR-DPVB *vs* DPVB, the exhausted and activated associated molecular have been highlighted. The threshold of the DEGs is $|\log_2 FC| > 0.25$, $P < 0.05$. Red = upregulated genes; blue = downregulated genes; gray = non-DEGs. **(b)** Heatmaps of the exhausted and activated associated molecular depicting gene expression patterns across the LR-DPVB and DPVB groups in Hepa1-6 HCC tumor. **(c)** Dot gram representing the expression of various exhausted and effected function markers in CD8_T subsets in Hepa1-6 HCC tumor of indicated group. **(d)** Bubble chart of DEGs pathway enrichment of CD8_T cells in Hepa1-6 HCC tumor with LR-DPVB and DPVB groups. **(e-f)** Representative flow cytometry plots **(e)** and quantification **(f)** of % PD-1^+ in $CD8^+$ T cells of Hepa1-6 HCC tumor in indicated groups. **(g-h)** Representative flow cytometry plots **(g)** and quantification **(h)** of % $Prf1^+$, % $Gzmb^+$, % Tnf-α^+ and % Ifn-γ^+ in $CD8^+$ T cells of Hepa1-6 HCC tumor in indicated groups. Data of **(f)** and **(h)** shown as means ± SD derived from tumor mouse models (n=3 mice/group). *P* values of **(f)** and **(h)** were calculated using a two-sided unpaired Student's *t* test. **(a-d)** n=3 mice/group. Source data are provided as a Source Data file.

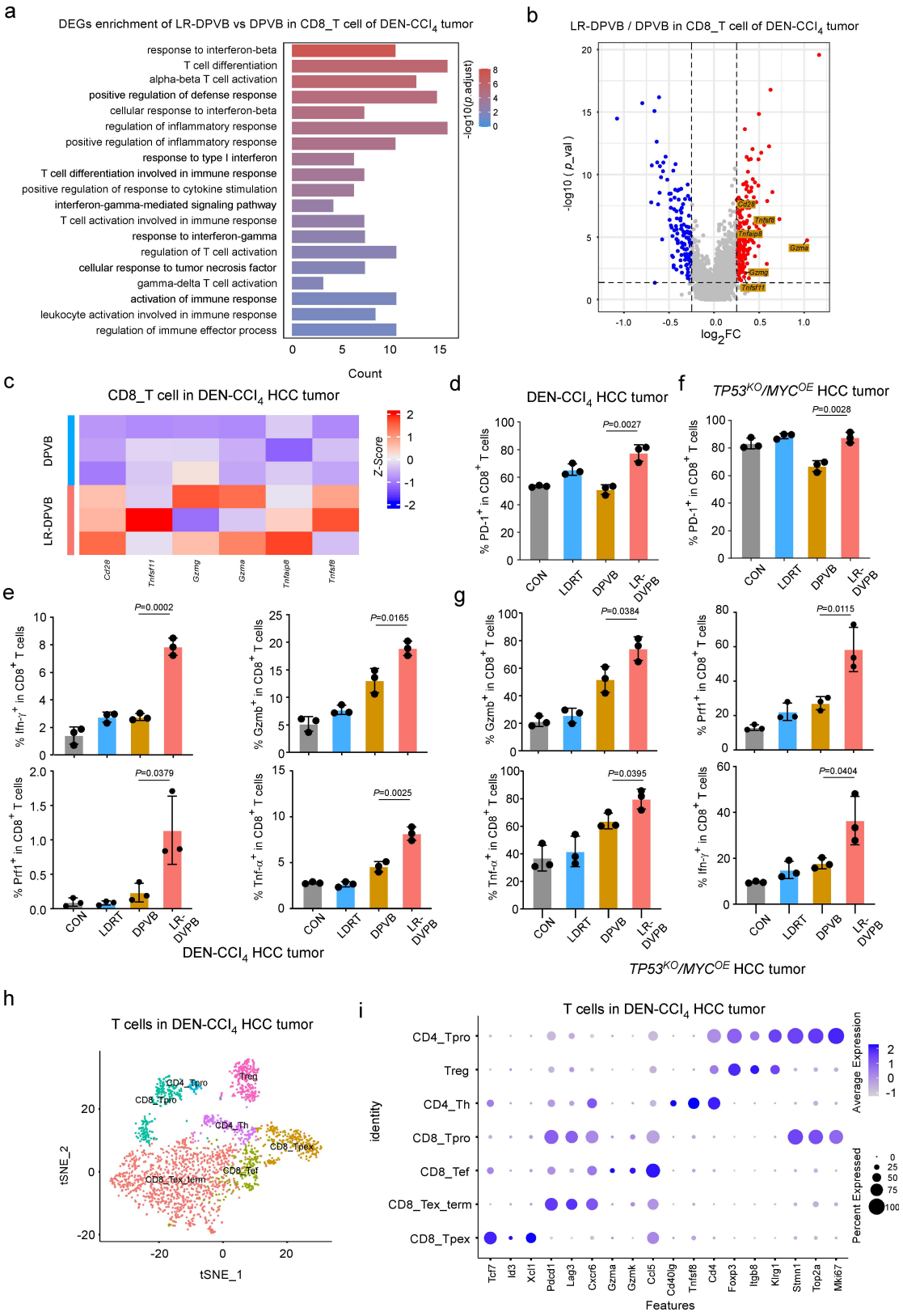

Supplementary Fig. 5 LR-DPVB enlarged the effector function and cytolytic capacity of tumor-rejecting CD8_T cell in DEN+CCl$_4$ HCC tumors and *Trp53^{KO}/MYC^{OE}* HCC tumors.

(a) Bar chart of DEGs pathway enrichment of CD8_T cell in DEN+CCl$_4$ HCC tumor

with LR-DPVB and DPVB groups. **(b-c)** Vocano map **(b)** and heatmap **(c)** of the activated associated molecular depicting gene expression patterns in CD8_T cell across the LR-DPVB and DPVB groups in DEN+CCl_4 HCC tumor. **(d)** Quantification of % PD-1^+ in $CD8^+$ T cells of DEN+CCl_4 HCC tumor in indicated groups. **(e)** Quantification of% $Prf1^+$, % $Gzmb^+$, % Tnf-α^+ and % Ifn-γ^+ in $CD8^+$ T cells of DEN+CCl_4 HCC tumor in indicated groups. **(f)** Quantification of % PD-1^+ in $CD8^+$ T cells of *Trp53*^{KO}/*MYC*^{OE} HCC tumor in indicated groups. **(g)** Quantification of% $Prf1^+$, % $Gzmb^+$, % Tnf-α^+ and % Ifn-γ^+ in $CD8^+$ T cells of *Trp53*^{KO}/*MYC*^{OE} HCC tumor in indicated groups. **(h)** tSNE maps of scRNAseq data of T cell from DEN+CCl_4 HCC tumor (n=3 tumors per group). CD4_Tpro = proliferating CD4_T cell, Treg = CD4_Treg, CD4_Th = helper CD4_T cell, CD8_Tpro = proliferating CD8_T cell, CD8_Tef = transient effected CD8_T cell, CD8_Tex_term = terminally exhausted CD8_T cell, CD8_Tpex = progenitor exhausted CD8_T cell. **(i)** DEN+CCl_4 HCC tumor T cells expressing indicated genes across major cell subsets and their corresponding average expression (size of dot indicates the percentage of cells in each population; expression intensity is indicated by color). **(a-c)** n=3 mice/group. Data of **(d-g)** shown as means ± SD derived from tumor mouse models (n=3 mice/group). *P* values of **(d-g)** were calculated using a two-sided unpaired Student's *t* test. Source data are provided as a Source Data file.

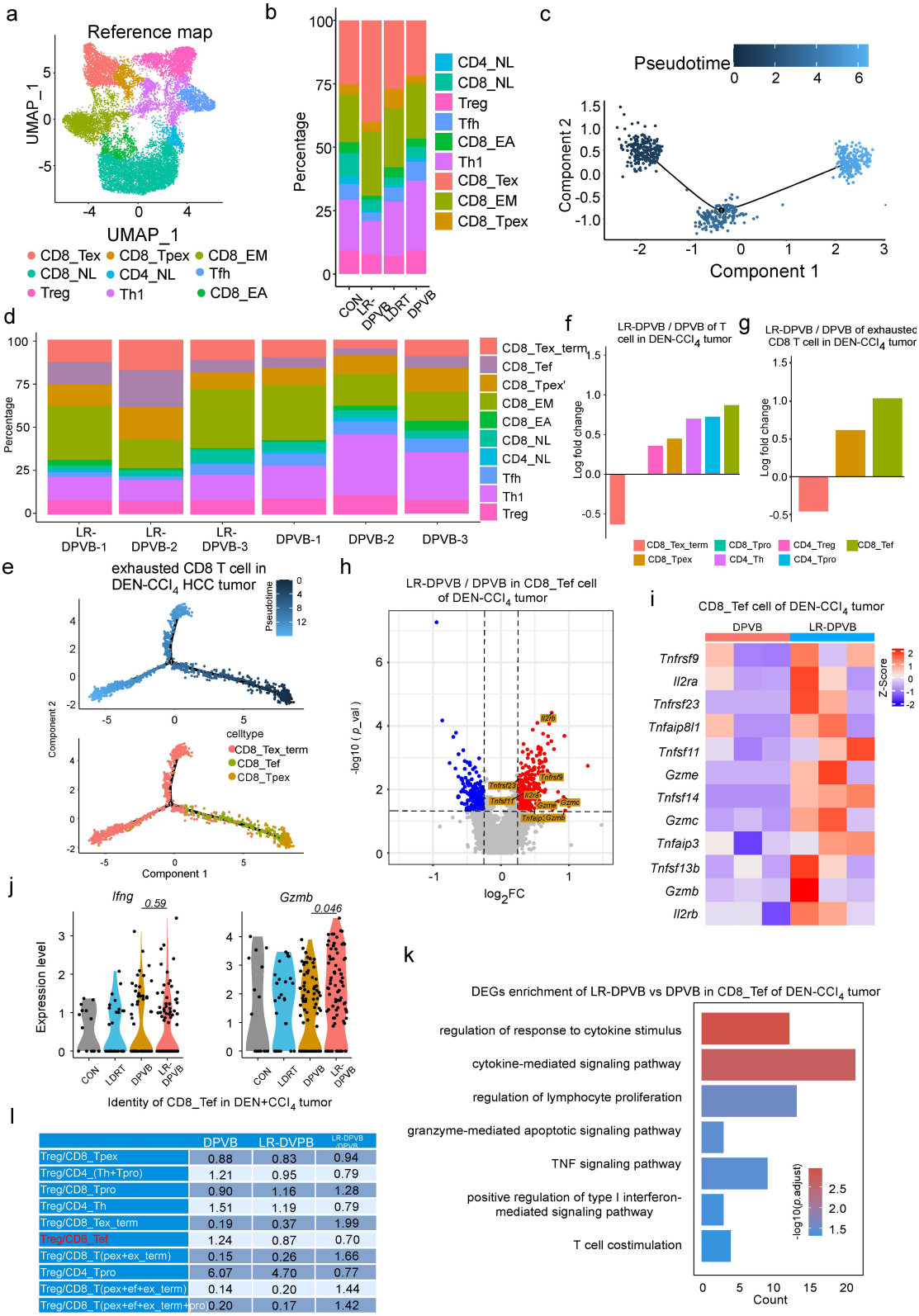

l

	DPVB	LR-DVPB	LR-DPVB /DPVB
Treg/CD8_Tpex	0.88	0.83	0.94
Treg/CD4_(Th+Tpro)	1.21	0.95	0.79
Treg/CD8_Tpro	0.90	1.16	1.28
Treg/CD4_Th	1.51	1.19	0.79
Treg/CD8_Tex_term	0.19	0.37	1.99
Treg/CD8_Tef	1.24	0.87	0.70
Treg/CD8_T(pex+ex_term)	0.15	0.26	1.66
Treg/CD4_Tpro	6.07	4.70	0.77
Treg/CD8_T(pex+ef+ex_term)	0.14	0.20	1.44
Treg/CD8_T(pex+ef+ex_term+pro)	0.20	0.17	1.42

Supplementary Fig. 6 The LR-DPVB expands the transitory effected CD8$^+$ T cells (CD8_Tef) featured a dramatic enrichment of effector function and cytolytic capacity.

(a) Reference map of UMAP plots of T cells scRNA-seq data (n=3 Hepa1-6 HCC

tumors per treatment). **(b)** Percentage stack plot representing the proportion of each cell subsets in different groups of Hepa1-6 HCC tumor. **(c)** Pseudotime trajectory analysis of CD8_Tpex and CD8_Tex clusters in Hepa1-6 was performed by the Monocle tool. **(d)** Percentage stack plot representing the proportion of each cell subsets in individual Hepa1-6 HCC tumor (no.1-3) from LR-DPVB or DPVB. (e) Pseudotime trajectory analysis of CD8_Tpex, CD8_Tef and CD8_Tex_term clusters of DEN+CCI_4 HCC tumor was performed by the Monocle tool. **(f)** Fold-change of T cell subsets of DEN+CCI_4 HCC tumor following LR-DPVB vs DPVB. **(g)** Fold-change of CD8_Tex subsets of DEN+CCI_4 HCC tumor following LR-DPVB vs DPVB. **(h-i)** Vocano map **(h)** and heatmap **(i)** of the activated associated molecular depicting gene expression patterns in CD8_Tef across the LR-DPVB and DPVB groups in DEN+CCI_4 HCC tumor. **(j)** Violin plot representing the expression of various exhausted and effected function markers in CD8_Tef subsets in DEN+CCI_4 HCC tumor of indicated group. **(k)** Bar chart of DEGs pathway enrichment of CD8_Tef cell in DEN+CCI_4 HCC tumor with LR-DPVB and DPVB groups. **(l)** Table describes Treg: CD8 or CD4 ratios in DEN+CCI_4 HCC tumor of LR-DPVB and DPVB groups.

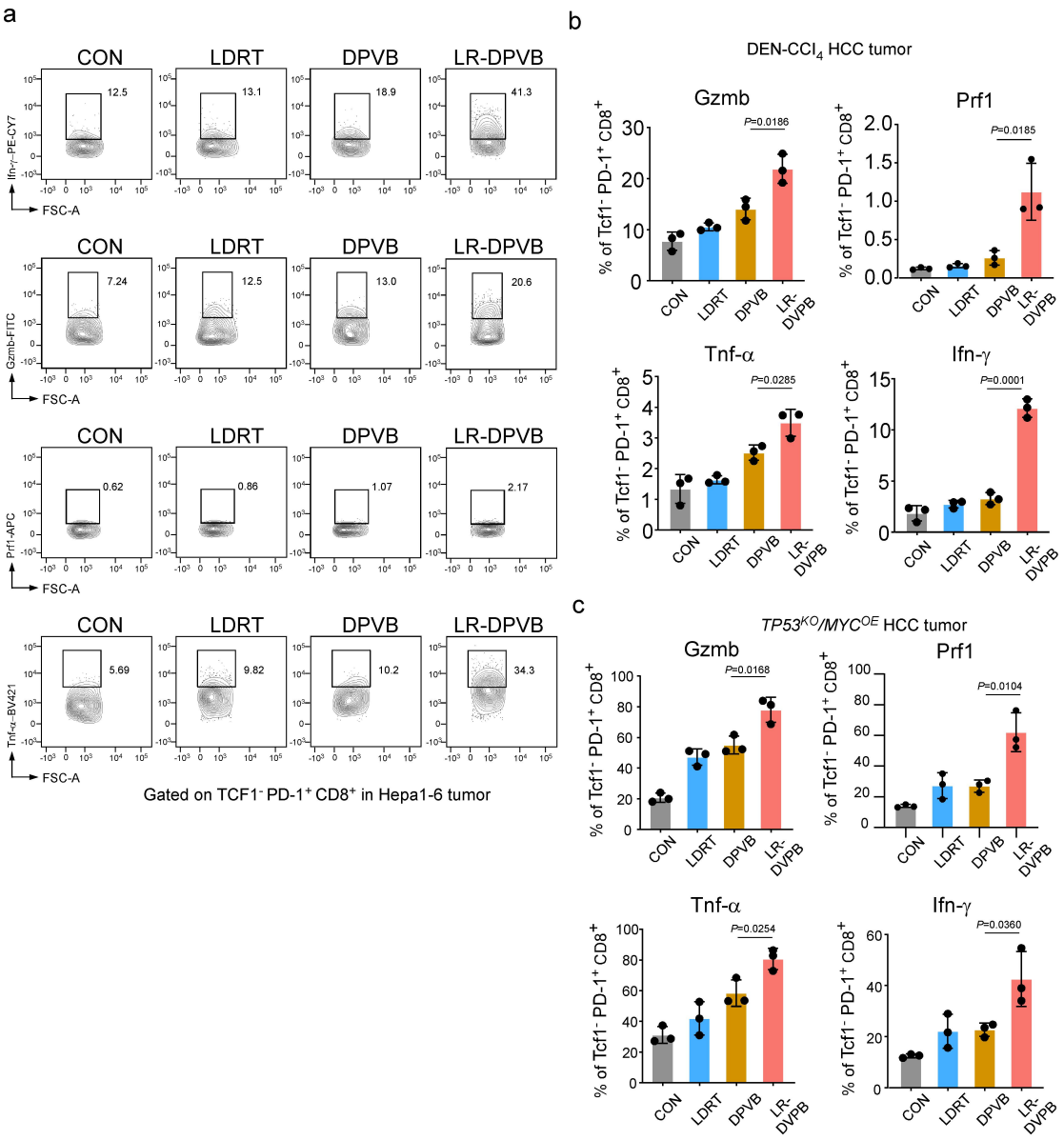

Supplementary Fig. 7 The flow cytometry assays of intratumoral CD8_Tef in three HCC models.

(a) Representative flow cytometry plots of % Prf1$^+$, % Gzmb$^+$, % Tnf-α$^+$ and % Ifn-γ$^+$ in TCF1$^-$ PD-1$^+$ CD8$^+$ T cells of Hepa1-6 tumor in the indicated groups. **(b)** Quantification of flow cytometry plots of % Prf1$^+$, % Gzmb$^+$, % Tnf-α$^+$ and % Ifn-γ$^+$ in TCF1$^-$ PD-1$^+$ CD8$^+$ T cells of DEN+CCl$_4$ HCC tumor in the indicated groups. **(c)** Quantification of flow cytometry plots of % Prf1$^+$, % Gzmb$^+$, % Tnf-α$^+$ and % Ifn-γ$^+$ in TCF1$^-$ PD-1$^+$ CD8$^+$ T cells of *Trp53^{KO}/MYC^{OE}* HCC tumors in the indicated groups. Data of **(b-c)** shown as means ± SD derived from tumor mouse models (n=3 mice/group). *P* values of **(b-c)** were calculated using a two-sided unpaired Student's *t*

test. Source data are provided as a Source Data file.

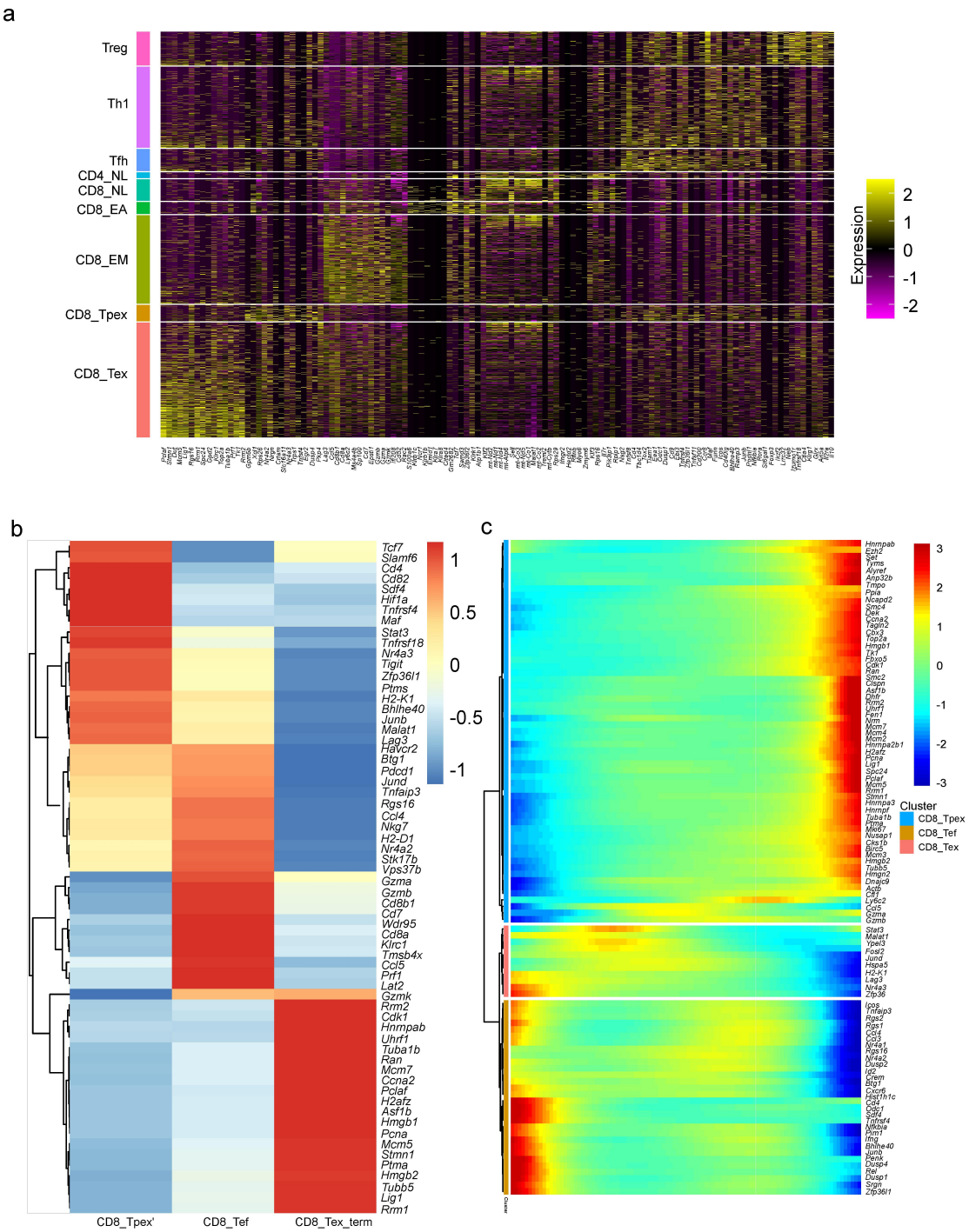

Supplementary Fig. 8 Phenotypic characterization of intratumoral T cells.

(a) The FindAllMarker function was used to calculate the tag genes of the classified cells, and the heatmap showed the top 15 tag genes of each subset. **(b)** The heatmap shows the characteristic genes of three cell subsets on the pseudotime trajectory. **(c)** The heatmap presents the top 100 genes associated with the pseudotime trajectory. **(a-c)** n=3 mice/group.

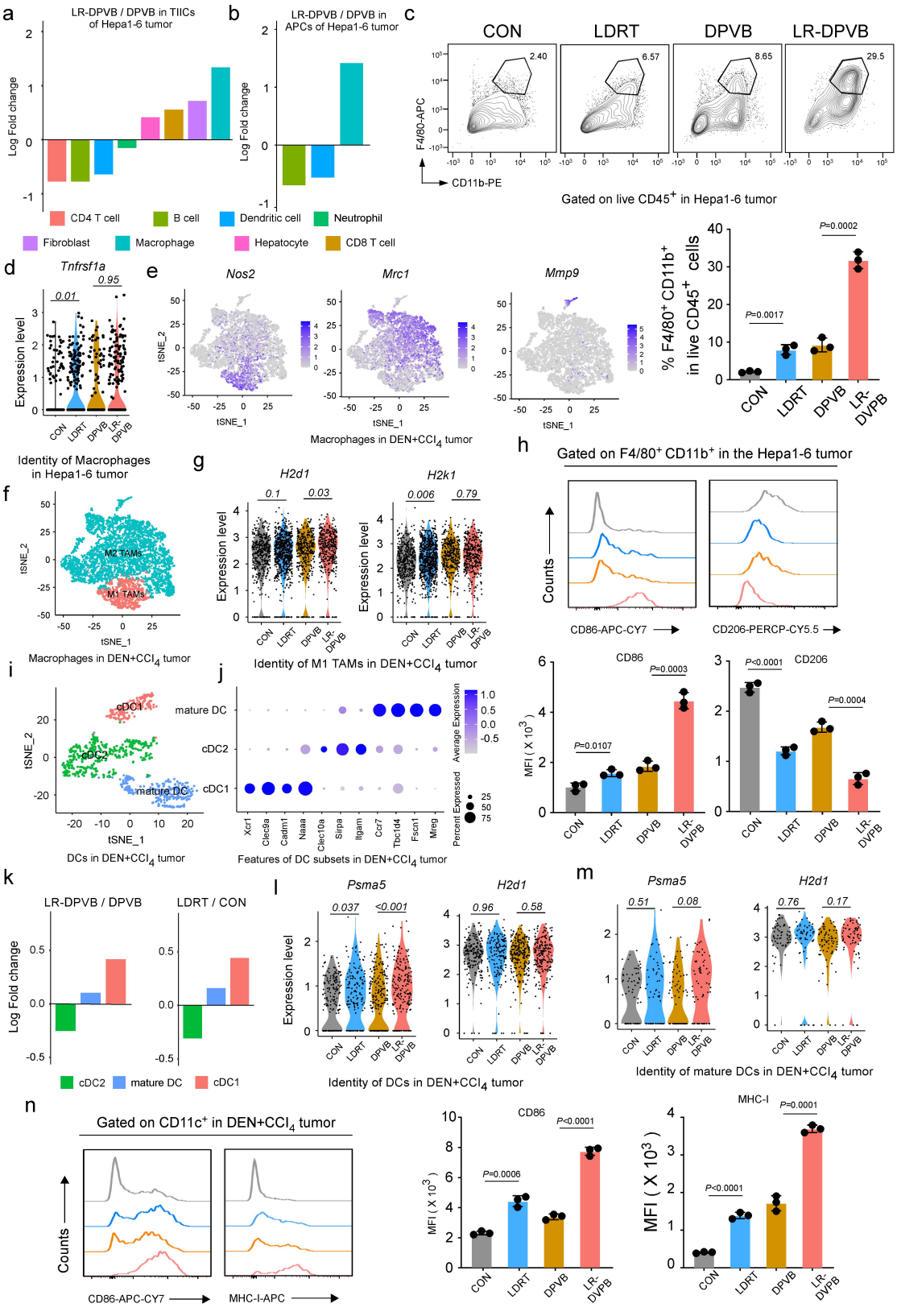

Supplementary Fig. 9 LR-DPVB effectively enhanced the activation of the tumor's innate immune microenvironment.

(a) Fold-change of TIICs populations from LR-DPVB and DPVB groups in Hepa1-6 HCC tumor. **(b)** Fold-change of antigen presented cell populations (APCs) from

LR-DPVB and DPVB groups in Hepa1-6 HCC tumor. **(c)** Representative (up panel) and quantification (down panel) of flow cytometry plots of % F4/80$^+$ CD11b$^+$ in live CD45$^+$ cells of Hepa1-6 HCC tumor TIICs at the end of the therapeutic cycle. **(d)** Violin plots representing the expression of *Tnfrsf1a* in macrophage subsets of Hepa1-6 HCC tumor with indicated treatment. **(e)** tSNE map of the indicated marker in macrophages of DEN+CCI_4 tumor. **(f)** tSNE map of the M1-type and M2-type macrophages of DEN+CCI_4 tumor. **(g)** Violin plots representing the expression of *H2d1* and *H2k1* in M1-type tumor-associated macrophage (TAMs) of DEN+CCI_4 tumor with indicated treatment. **(h)** Expression of CD86 and CD206 of F4/80$^+$ CD11b$^+$ cells in the Hepa1-6 HCC tumor with indicated treatment. Data shown as means ± SD of three independent experiments. **(i)** tSNE maps of scRNAseq data from DCs of DEN+CCI_4 tumor (n=3 per group). **(j)** DCs expressing indicated genes across major cell populations and their corresponding average expression (size of dot indicates the percentage of cells in each population; expression intensity is indicated by color). **(k)** Fold-change of DCs populations from LR-DPVB and DPVB groups (left panel) and LDRT and CON groups (right panel) in DEN+CCI_4 tumor. **(l-m)** Violin plots representing the expression of *Psma5* and *H2d1* in DCs **(l)** and mature DCs **(m)** of DEN+CCI_4 tumor with indicated treatment. **(n)** Expression of CD86 and MHC-I of CD11c$^+$ cells in the Hepa1-6 HCC tumor with indicated treatment. **(a-n)** n=3 mice/group. Data of **(c)**, **(h)** and **(n)** shown as means ± SD derived from tumor mouse models (n=3 mice/group). *P* values of **(c)**, **(h)** and **(n)** were calculated using a two-sided unpaired Student's *t* test. Source data are provided as a Source Data file.

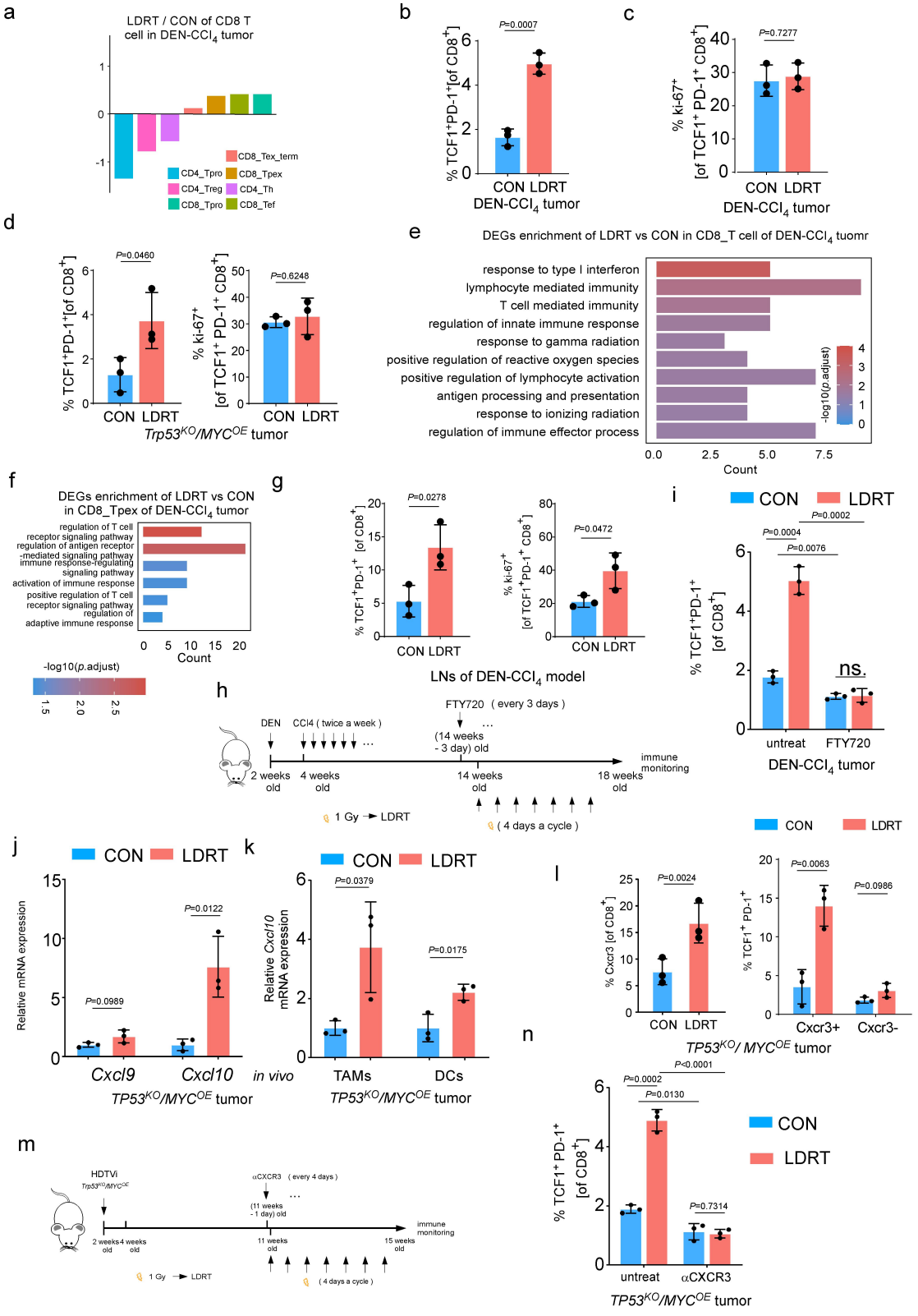

Supplementary Fig. 10 LDRT-induced intratumoral stem-like CD8_Tpex was recruited from the dLNs through by CXCL10/CXCR3 axis.

(a) Fold-change of T cell subsets following LDRT vs CON in DEN+CCl4 model. n=3 mice/group. **(b-c)** Flow cytometry quantification of % TCF1$^+$ PD-1$^+$ in CD8$^+$ T cells

and % Ki-67$^+$ in TCF1$^+$ PD-1$^+$ CD8$^+$ T cells of the indicated groups in DEN-CCl_4 model. **(d)** Flow cytometry quantification of % TCF1$^+$ PD-1$^+$ in CD8$^+$ T cells (left panel) and % Ki-67$^+$ in TCF1$^+$ PD-1$^+$ CD8$^+$ T cells (right panel) of the indicated groups in *Trp53^{KO}/MYC^{OE}* model. **(e)** Bar chart of DEGs pathway enrichment of CD8_T cell in DEN+CCl_4 HCC tumor with LDRT and CON groups. n=3 mice/group. **(f)** Bar chart of DEGs pathway enrichment of CD8_Tpex in DEN+CCl_4 HCC tumor with LR-DPVB and DPVB groups. n=3 mice/group. **(g)** Flow cytometry quantification of % TCF1$^+$ PD-1$^+$ in CD8$^+$ T cells and % Ki-67$^+$ in TCF1$^+$ PD-1$^+$ CD8$^+$ T cells of the dLNs of indicated groups in DEN-CCl_4 model. **(h-i)** Schematic FTY720 in DEN-CCl_4 LDRT treated mice **(h)** and quantification of % TCF1$^+$ PD-1$^+$ in CD8$^+$ T cells in the tumors of the indicated groups **(i)**. **(j)** Relative mRNA expression of *Cxcl9* and *Cxcl10* in LDRT and CON groups of *Trp53^{KO}/MYC^{OE}* tumor tissue. **(k)** Relative mRNA expression of *Cxcl10* in LDRT and CON groups of tumor-associated macrophages (TAMs, F4/80+ CD11b$^+$ CD45$^+$ L/D$^-$) and DCs (CD11c$^+$ CD45$^+$ L/D$^-$) cells sorted from tumor-infiltrated immune cells (TIICs) of *Trp53^{KO}/MYC^{OE}* tumor. **(l)** Quantification flow cytometry of % CXCR3$^+$ in CD8$^+$ T cells (left panel), % TCF1$^+$ PD-1$^+$ in CXCR3$^+$ CD8$^+$ T cells and CXCR3$^-$ CD8$^+$ T cells (right panel) in the *Trp53^{KO}/MYC^{OE}* tumors of the indicated groups. **(m-n)** Schematic depiction of anti-CXCR3 in LDRT-treated *Trp53^{KO}/MYC^{OE}* mice **(m)** and quantification of % TCF1$^+$ PD-1$^+$ in CD8$^+$ T cells in the tumors of the indicated groups **(n)**. Data of **(b-d)**, **(g)**, **(i-l)** and **(n)** shown as means ± SD derived from tumor mouse models (n=3 mice/group). *P* values of **(b-d)**, **(g)**, **(i-l)** and **(n)** were calculated using a two-sided unpaired Student's *t* test. Source data are provided as a Source Data file.

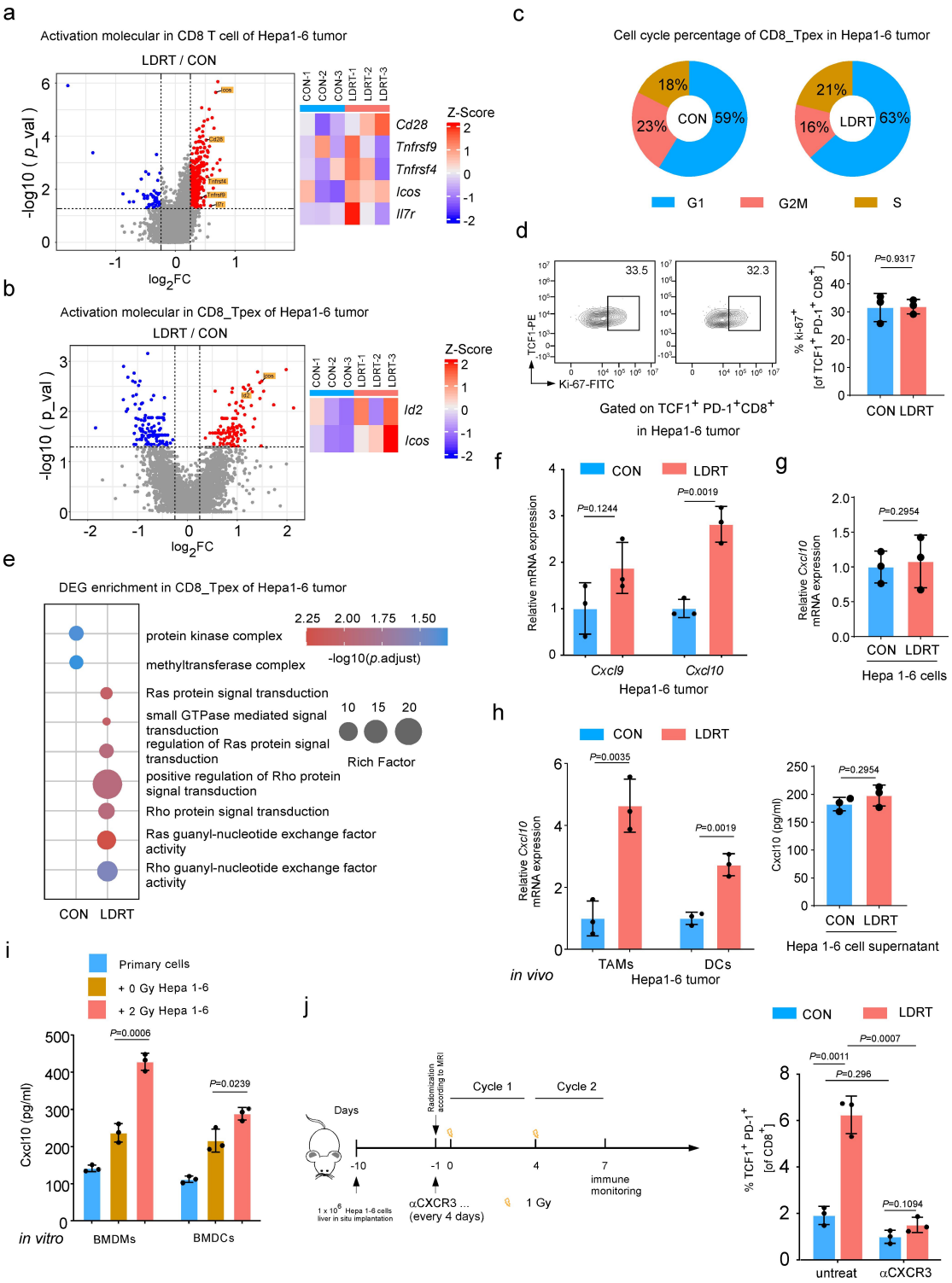

Supplementary Fig. 11 Role of peripheral lymphatic trafficking in intratumoral stem-like CD8$^+$ Tpex accumulation via CXCL10/CXCR3 axis.

(a-b) Volcano plot representing the DEGs of LDRT vs CON in CD8 T cell **(a)** and CD8_Tpex **(b)**, the activation molecular have been highlighted (left panel). The threshold of the DEGs is $|\log_2FC|>0.25$, $P<0.05$. Red = upregulated genes; blue = downregulated genes; gray = non-DEGs. Heatmaps (right panel) of the activation

molecular depicting gene expression patterns across the LDRT and CON groups in $CD8^+$ T cells **(a)** and CD8_Tpex **(b)**. n=3 mice/group. **(c)** Pie chart depicting the % of the cell cycle of CD8_Tpex in LDRT and CON groups. n=3 mice/group. **(d)** Representative flow cytometry plots (left panel) and quantification (right panel) of % Ki-67^+ in $TCF1^+$ PD-1^+ $CD8^+$ T cells of the indicated groups. **(e)** Bubble chart of DEG pathway enrichment of CD8_Tpex in LDRT and CON groups. n=3 mice/group. **(f)** Relative mRNA expression of *Cxcl9* and *Cxcl10* in LDRT and CON groups of Hepa1-6 tumor tissue. **(g)** Relative mRNA expression of *Cxcl10* in Hepa1-6 cells (up panel) and protein level of of Cxcl10 of supernatant of Hepa1-6 cells in LDRT and CON groups (down panel). **(h)** Relative mRNA expression of *Cxcl10* in LDRT and CON groups of tumor-associated macrophages (TAMs, F4/80+ $CD11b^+$ $CD45^+$ L/D^-) and DCs ($CD11c^+$ $CD45^+$ L/D^-) cells sorted from tumor-infiltrated immune cells (TIICs). **(i)** The protein level of of Cxcl10 of supernatant of the indicated groups of *in vitro* co-culture assays. **(j)** Schematic depiction of anti-CXCR3 in Hepa1-6 bearing LDRT treated mice (up panel) and quantification of % $TCF1^+$ PD-1^+ in $CD8^+$ T cells in the tumors of the indicated groups (down panel). Data of **(d)**, **(f)**, **(h)** and **(j)** shown as means ± SD derived from tumor mouse models (n=3 mice/group). Data of **(g)** and **(i)** shown as means ± SD of 3 independent biological experiments. *P* values of **(d)** and **(f-j)** were calculated using a two-sided unpaired Student's *t* test. Source data are provided as a Source Data file.

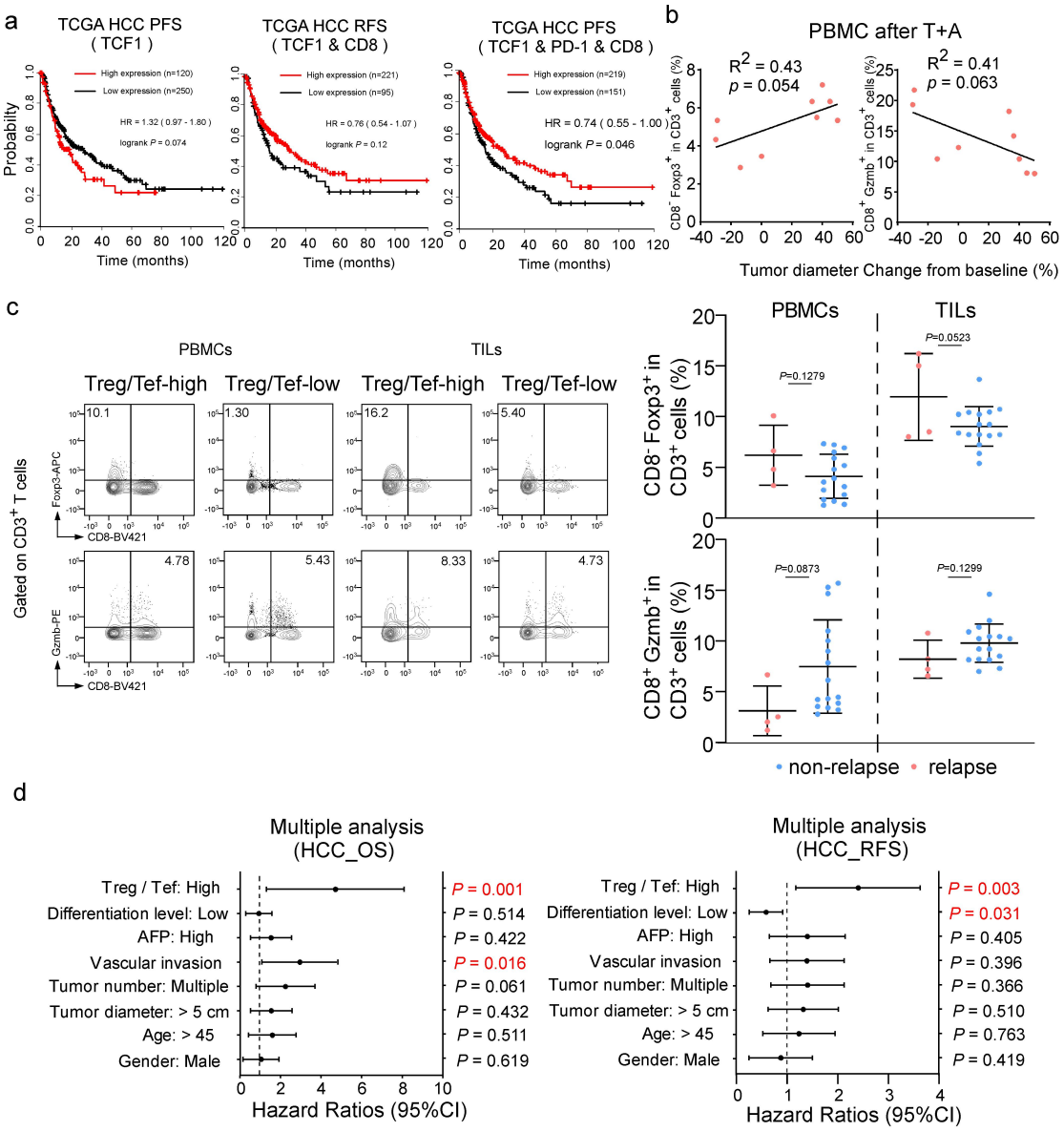

Supplementary Fig. 12 Low infiltration of stem-like CD8$^+$ Tpex and high Treg/Tef ratio correlates with poor prognosis in HCC.

(a) The Kaplan–Meier Plotter (http://kmplot.com/analysis) program was used to analyze the infiltration of stem-like CD8+ Tpex in progress-free survival (PFS) of HCC. **(b)** Graphs depict correlation between the tumor diameter change from baseline (%) and Treg (%) or Tef (%). *P* value and R^2 value were calculated using linear regression analysis (n=9). **(c)** Representative flow cytometry plots (left panel) and quantification (right panel) of Treg/Tef of PBMC or TIICs in the indicated HCC groups. Relapse: n=4. non-relapse: n=16. *P* values were calculated using a two-sided unpaired Student's *t* test. Data of shown as means ± SD. **(d)** Multivariate Cox

regression analysis to evaluate the significance of the association between the Treg/Tef signature of 5-year OS and 5-year RFS in the presence of other clinical variables. Source data are provided as a Source Data file.

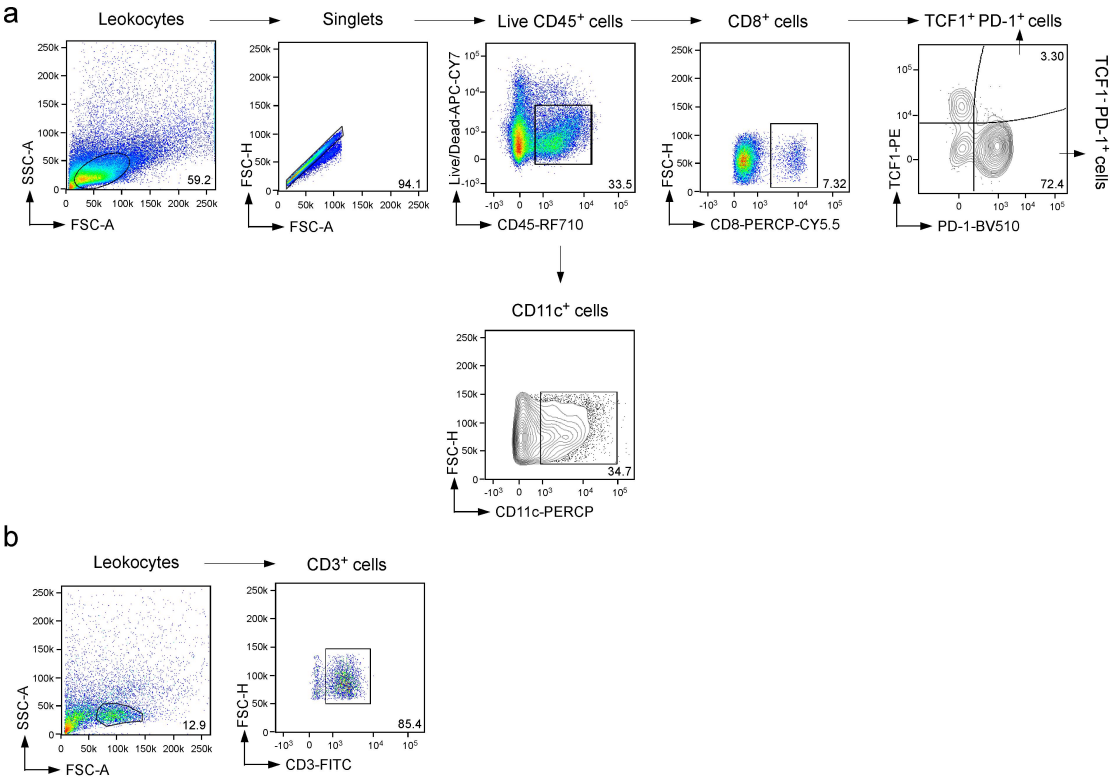

Supplementary Fig. 13 Gating strategy.

(a) Gating strategy used in Fig. 2, 4, 5, 7 and Supplementary Fig. 4, 5, 7, 9-11. **(b)** Gating strategy used in Fig. 7 and Supplementary Fig. 12.

Supplementary Tables:

Supplementary Table 1. Clinical information of HCC patients with T+A treatment.

patient No.	$TCF1^+$ $PD1^+$ $CD8^+$ /$CD8^+$ cells (%)	Therapeutic effect of T+A
1	4.16	PR
2	8.3	PR
3	10	PR
4	2.72	SD
5	2	SD
6	1.25	PD
7	1.76	PD
8	3	SD
9	2.67	SD

Supplementary Table 2. Clinical information of HCC patients with T+A treatment.

patient No.	Therapeutic effect of T+A	change from baseline	Treg (%) in PBMC	Tef (%） in PBMC	Treg/Tef in PBMC
1	PR	-30%	5.35	8.03	0.666251557
2	PD	50%	6.35	8.12	0.782019704
3	SD	-14%	7.21	10.45	0.689952153
4	PD	36.40%	5.51	14.21	0.387755102
5	PD	40%	6.35	18.24	0.348135965
6	PD	33.30%	3.46	12.29	0.281529699
7	PD	45%	2.88	10.45	0.275598086
8	PR	-29.10%	5.35	21.75	0.245977011
9	PD	0%	4.34	19.35	0.224289406

Supplementary Table 3. Clinical information of primary HCC with surgical resection.

patient No.	recurrence status within 6 months	Treg (%) in PBMCs	Tef (%) in PBMCs	Treg/Tef in PBMCs	Treg (%) in TIICs	Tef (%) in TIICs	Treg/Tef in TIICs
1	0	1.69	4.49	0.38	6.36	8.16	0.78
2	0	6.52	9.01	0.72	5.4	8.16	0.66
3	0	3.94	15.7	0.25	8.37	7.33	1.14
4	1	10.1	6.68	1.51	8.51	8.25	1.03
5	0	3.12	14.7	0.21	10.22	9.23	1.11
6	0	1.29	3.45	0.37	8.12	8.23	0.99
7	0	1.37	3.57	0.38	9.23	9.23	1.00
8	0	1.84	11	0.17	8.23	10.27	0.80
9	1	3.23	2.04	1.58	15	10.8	1.39
10	0	2.78	15.3	0.18	8.24	10.45	0.79
11	1	4.83	1.21	3.99	16.2	7.23	2.24
12	0	2.33	4.24	0.55	8.24	10.25	0.80
13	0	7.23	6.16	1.17	10.74	8.53	1.26
14	0	4.83	3.89	1.24	9.23	10.92	0.85
15	0	6.64	2.56	2.59	8.01	6.57	1.22
16	0	5.21	4.33	1.20	10.45	10.24	1.02
17	0	3.56	7.88	0.45	7.23	11.38	0.64
18	0	7.34	3.23	2.27	13.67	7.03	1.94
19	0	6.94	2.8	2.48	10.23	14.63	0.70
20	0	5.93	10.04	0.59	10.41	12.03	0.87

Supplementary Table 4. Clinicopathological characteristics of 120 patients with primary HCC.

Parameters	Number of cases (%)
Gender	
Male	103 (85.8)
Female	17 (14.2)
Age	
≤ 45	33 (27.5)
> 45	87 (72.5)
Tumor diameter	
≤ 5 cm	61 (50.8)
> 5 cm	59 (49.2)
Tumor number	
Single	81 (67.5)
Multiple	39 (32.5)
Vascular invasion	
No	70 (58.3)
Yes	50 (41.7)
AFP	
< 400 ng/ml	84 (70.0)
≥ 400 ng/ml	36 (30.0)
Degree of differentiation	
Intermediate and high	41 (34.1)
Low	79 (65.9)
5-years vital status	
Alive	78 (65)
Dead	42 (35)
Relapse status within 5 years	
No	52 (43.3)
Yes	68 (56.7)
Treg/Tef ratio level	
Low	60 (50.0)
High	60 (50.0)

Supplementary Table 5. Correlation between Treg/Tef and clinicopathological characteristics of patients with primary HCC.

Characteristics	Treg / Tef ratio level		*P* values
	Low, no. of cases	High, no. of cases	
Gender			
Male	51	52	0.793
Female	9	8	
Age			
≤ 45	19	14	0.307
> 45	41	46	
Tumor diameter			
≤ 5 cm	32	29	0.584
> 5 cm	28	31	
Tumor number			
Single	46	35	**0.032**
Multiple	14	25	
Vascular invasion			
No	39	31	0.139
Yes	21	29	
AFP			
< 400 ng/ml	45	39	0.232
≥ 400 ng/ml	15	21	
Degree of differentiation			
Intermediate and high	18	23	0.336
Low	42	37	
5-years vital status			
Alive	51	27	**<0.0001**
Dead	9	33	
Relapse status within 5 years			
No	34	18	**0.003**
Yes	26	42	

P values were calculated using two-sided χ^2 test.

Supplementary Table 6. Univariate and multivariate analysis of factors associated with 5-year overall survival in patients with primary HCC.

Characteristics	Univariate analysis		Multivariate analysis	
	HR (95% CI)	*P* values	HR (95% CI)	*P* values
Gender				
Male *vs.* Female	1.058 (0.446-2.511)	0.899	0.788 (0.307-2.020)	0.619
Age				
> 45 *vs.* ≤ 45	0.961 (0.492-1.877)	0.907	1.306 (0.589-2.892)	0.511
Tumor diameter				
> 5 cm *vs.* ≤ 5 cm	1.541 (0.836-2.841)	0.166	1.323 (0.658-2.658)	0.432
Tumor number				
Multiple *vs.* Single	2.178 (1.187-3.995)	**0.012**	1.928 (0.970-3.831)	0.061
Vascular invasion				
Yes *vs*. No	3.23 (1.716-6.081)	**<0.0001**	2.393 (1.180-4.856)	**0.016**
AFP				
≥ 400 ng/ml *vs.* < 400 ng/ml	2.209 (1.202-4.059)	**0.011**	1.314 (0.655-2.638)	0.422
Degree of differentiation				
Intermediate and high *vs.* Low	0.703 (0.306-.374)	0.303	0.782 (0.373-1.639)	0.514
Treg/Tef ratio level				
High *vs.* Low	4.915 (2.347-10.291)	**<0.0001**	3.888 (1.793-8.432)	**0.001**

HR, hazard ratio; CI, confidence interval; Statistical analyses were performed using the Cox regression model (two-sided Likelihood ratio test).

Supplementary Table 7. Univariate and multivariate analysis of factors associated with 5-year relapse-free survival in patients with primary HCC.

Characteristics	Univariate analysis		Multivariate analysis	
	HR (95% CI)	*P* values	HR (95% CI)	*P* values
Gender				
Male *vs.* Female	1.045 (0.518-2.108)	0.901	0.730 (0.341-1.564)	0.419
Age				
> 45 *vs.* ≤ 45	0.890 (0.524-1.511)	0.666	1.097 (0.601-2.004)	0.763
Tumor diameter				
> 5 cm *vs.* ≤ 5 cm	1.395 (0.866-2.248)	0.171	1.200 (0.698-2.061)	0.51
Tumor number				
Multiple *vs.* Single	1.502 (0.917-2.460)	0.106	1.280 (0.750-2.184)	0.366
Vascular invasion				
Yes *vs*. No	1.685 (1.046-2.715)	**0.032**	1.266 (0.734-2.182)	0.396
AFP				
≥ 400 ng/ml *vs.* < 400 ng/ml	1.615 (0.976-2.613)	0.062	1.266 (0.727-2.202)	0.405
Degree of differentiation				
Intermediate and high *vs.* Low	0.556 (0.327-0.945)	**0.03**	0.524 (0.291-0.943)	**0.031**
Treg/Tef ratio level				
High *vs.* Low	2.260 (1.384-3.691)	**0.001**	2.195 (1.295-3.720)	**0.003**

HR, hazard ratio; CI, confidence interval; Statistical analyses were performed using the Cox regression model (two-sided Likelihood ratio test).

Supplementary Table 8. The antibodies used in flow cytometry.

Antibody / Dye	Brand	Cat#	Dilutions	clone numbers
Ghost Dye Red780	TONBO Bioscience	13-0865-T100	1 ul/1 ml	NA
anti-mouse CD45-redFluor 710	TONBO Bioscience	80-0451-U100	0.25 μg per 10^6 cells in 100 μl	30-F11
anti-mouse CD4-APC	Biolegend	100411	0.25 μg per 10^6 cells in 100 μl	GK1.5
anti-mouse CD8-PerCP-Cy5.5	TONBO Bioscience	65-0081-U025	0.25 μg per 10^6 cells in 100 μl	53-6.7
anti-mouse TNF-α-BV421	Biolegend	506328	0.25 μg per 10^6 cells in 100 μl	MP6-XT22
anti-mouse PD-1-BV510	Biolegend	135241	0.25 μg per 10^6 cells in 100 μl	29F.1A12
anti-mouse KI-67-FITC	eBioscience	11-5698-80	0.25 μg per 10^6 cells in 100 μl	SolA15
anti-mouse CD11b-PE	Biolegend	101207	0.25 μg per 10^6 cells in 100 μl	M1/70
anti-mouse CD86-APC-CY7	Biolegend	105030	0.25 μg per 10^6 cells in 100 μl	GL-1
anti-mouse CD11c-PERCP	Biolegend	117325	0.25 μg per 10^6 cells in 100 μl	N418
anti-mouse MHC-I-APC	Biolegend	114713	0.25 μg per 10^6 cells in 100 μl	34-1-2S
anti-mouse IFN-γ-PE-Cy7	TONBO Bioscience	60-7311-U100	0.125 μg per 10^6 cells in 100 μl	XMG1.2
anti-mouse SLAMF6-PE	Biolegend	134606	1.0 μg per 10^6 cells in 100 μl	330-AJ
anti-mouse PRF1-APC	Invitrogen	17-9392-80	1.0 μg per 10^6 cells in 100 μl	17-9392-80

anti-mouse TCF1-PE	CST	14456S	1:50	C63D9
anti-mouse F4/80-APC	Biolegend	157306	0.5 μg per 10^6 cells in 100 μl	QA17A29
anti-mouse CD206-PERCP-CY5.5	Biolegend	141716	0.5 μg per 10^6 cells in 100 μl	C068C2
anti-mouse CXCR3-BV421	Biolegend	126521	0.5 μg per 10^6 cells in 100 μl	CXCR3-173
anti-mouse GZMB-FITC	Biolegend	372206	5 μl per 10^6 cells in 100 μl	QA16A02
anti-human CD3-FITC	Biolegend	317306	5 μl per 10^6 cells in 100 μl	OKT3
anti-human CD8-BV421	Biolegend	301035	5 μl per 10^6 cells in 100 μl	RPA-T8
anti-human GZMB-PE	eBioscience	12-8899-41	5 μl per 10^6 cells in 100 μl	GB11
anti-human FOXP3-APC	eBioscience	17-4776-42	5 μl per 10^6 cells in 100 μl	1704776-42
anti-human PD-1-PERCP	Biolegend	329937	5 μl per 10^6 cells in 100 μl	EH12.2H7
anti-human TCF1-PE	Biolegend	655208	5 μl per 10^6 cells in 100 μl	7F11A10